Local temporal variability reflects functional network integration in the human brain: On the crucial role of the thalamus

Douglas D. Garrett[1,2], Samira M. Epp[1,2], & Ulman Lindenberger[1,2]

[1]Max Planck UCL Centre for Computational Psychiatry and Ageing Research, Berlin/London; [2]Center for Lifespan Psychology, Max Planck Institute for Human Development, Lentzeallee 94, 14195 Berlin, Germany.

Corresponding author: Douglas D. Garrett, Max Planck UCL Centre for Computational Psychiatry and Ageing Research, Center for Lifespan Psychology, Max Planck Institute for Human Development, Lentzeallee 94, 14195 Berlin, Germany. Tel.: +49-30-824-06-216, garrett@mpib-berlin.mpg.de.

Keywords: brain signal variability; neural dynamics; network dimensionality; fMRI.

Manuscript information: 34 pages, 2 tables, 3 figures, 4 SI tables, 7 SI figures

Abstract

Local moment-to-moment variability exists at every level of neural organization, but its driving forces remain opaque. Based on animal work showing that within-region variability can be a primary function of synaptic input, we used fMRI to test in humans whether greater temporal variability in local brain regions was associated with higher functional network integration. We found that individuals with higher local temporal variability had a more integrated (lower-dimensional) network fingerprint, with temporal variability in the thalamus showing the strongest association with network dimensionality. Beyond animal findings showing that local variability should upregulate from thalamus to visual cortex, we found that local variability upregulated from thalamus to all structurally connected cortical targets. Critically, greater within-person thalamo-cortical upregulation was associated with higher integration in 12 of 13 examined networks. Our findings indicate that local variability primarily reflects functional integration, with the thalamus acting as a relay or modulator of variability in cortex.

Local variability reflects lower dimensional functional integration in the human brain

The human brain is remarkably variable across moments, exhibiting multiple dynamic signatures (e.g., variance, nonstationarity) at every level of neural function[1]. The field of cognitive neuroscience has increasingly examined the predictive utility of brain signal variability for understanding broad-scale individual differences in human brain function (e.g., predicting age, cognitive performance, disease status), an approach that continues to gain traction, yet remains grossly understudied[2]. In particular, the nature and driving forces of temporal variability are rather opaque, with several competing definitions and associated theories[2]. Logically, if dynamic neural activity at the regional level (in animals) is indeed a primary function of its synaptic inputs[3], then one simple starting point is to investigate how local temporal variability in the human brain may may relate to functional connectivity[4]. Interestingly, the direction and manifestation of this potential relationship is not trivial.

Theoretically, high local signal variability could result from highly disparate functional network scenarios. For example, (i) via a lower dimensional, well-integrated functional network composition, local variability would be a function of a coherent and common "drive" among a greater number of network regions. Accordingly, the dynamic range of a local brain signal would result from heightened levels of synchronized processes across connected regions, regardless of whether those processes are deterministic or stochastic (they must only be shared). Further, with a greater number of functional inputs to any local region that may operate across moments[1], the probability of variable functional output may also increase. Conversely, high local variability could also conceivably result from (ii) a more fractionated (higher dimensional) network system. Here, greater local moment-to-moment fluctuations may be due to a lack of "entrainment" by a reduced number of available functional inputs (and thus, likely driven more by local sources of stochasticity); accordingly, local variability could therefore represent a lack of coordinated information transfer in the brain. In light of theories suggesting that more disconnected, fractionated biological systems are less dynamic across moments[5], alternative (i) may be more likely. Critically, animal and computational work focusing primarily on visual cortex has shown that local fluctuations in brain output can be directly attributed to momentary variations in synaptic input, rather than some unknown source of local noise[3], and, remarkably, the majority of apparent "noise variation" is shared across neurons that are similarly functionally tuned[6-8]. These features suggest a plausible general phenomenon that could also apply to the human brain – that more temporal variability at the regional level may be characterized by a lower dimensional network fingerprint.

The thalamus may play a key role in the relation between local variability and brain-wide network dimensionality. The thalamus maintains projections to the entire cortex and is thought to either relay and/or modulate information flow throughout the entire brain[9,10]. To the extent that temporal variability is indeed an expression of information flow or "dynamic range"[2], thalamic variability may provide a key temporal signature of whole-brain network dimensionality. Further, it has been demonstrated that macaque[8] and cat visual cortex[6,11] may inherit and then upregulate temporal variability explicitly from thalamic inputs. However, such upregulation from thalamus to visual cortex has not yet been demonstrated in humans, nor expanded to examine links between thalamic temporal variability and that of the broader cortex to which it connects. Further, it remains unknown the extent to which within-person upregulation of temporal variability from thalamus to cortex reflects network integration via network dimensionality. We have posed previously that the brain's ability to modulate variability levels within-person (across task conditions) provides a key signature of neural "degrees of freedom" in response to differential environmental demands[2,12,13]. Should the thalamus indeed be considered a dynamic and integrative "pacemaker" for the brain, then

thalamic variability may provide a key temporal signature of lower network dimensionality. In addition, between-person differences in within-person upregulation of signal variability from thalamus to cortex should also be associated with lower network dimensionality; if so, the thalamus would qualify as a key region linking locally assessed brain signal variability to network dimensionality overall.

In the present study, we examined high speed, multiband fMRI resting-state data (10 mins, TR=645ms) within the publicly available NKI-Enhanced dataset (N = 100, 18–85 years)[14]. Our goals were to test the hypothesis that moment-to-moment variability in voxel-wise brain signals reflects lower dimensional network integration at the individual level, and to examine the role of the thalamus in this association. Prior to model runs, within-voxel temporal variability was estimated by taking the square root of the Fourier power (summed over .01–.10 Hz; akin to taking the standard deviation over the same bandpass filtered signal). Network dimensionality was estimated primarily using spatial principal components analysis (PCA; see Methods and Results for other alternative approaches also examined); using each participant's spatiotemporal matrix, we counted the number of PCA dimensions required to capture 90% of the correlations across regions in each subject's brain. Notably, this within-person network dimensionality approach allowed us to capture individual differences in functional network composition, which could then be related to local voxel-wise temporal fluctuations, within-person.

Results

Whole-brain model

In line with our initial hypothesis, multivariate partial least squares (PLS) modeling (see Methods) revealed that greater local temporal fluctuations coincided with lower network dimensionality (r = –0.84 (95% bootstrap confidence interval (CI) = –.81, –.88); $p = 2.22*10^{-27}$). Spatially, this was a robust and global phenomenon at typical threshold levels (see Figure 1). When increasing statistical thresholds greatly (see Figure 1), temporal variability in bilateral thalamus was indeed the peak correlate of lower whole-brain network dimensionality. A series of control analyses demonstrated that this negative relation between local variability and network dimensionality held independent of adult age, specific power band (i.e., low, medium, or high frequency), or method of dimensionality estimation method (i.e., correlation matrix-based PCA, covariance-based PCA, or independent components analysis; see Supplementary Results, Table S1, and Figures S1 and S2).

Our primary finding thus demonstrates a negative relation between PCA dimensionality and local signal variability. Prior to estimation of more specific models (see below), it is important to consider that the statistical conditions required for this negative relation to emerge are non-trivial. If we consider the correlation formula that provides the initial matrix for PCA decomposition,

$$r = \frac{\sum(x_i - \bar{x})\,(y_i - \bar{y})}{SD_x SD_y}$$

the between-region time series covariance (numerator) is scaled by the time series' standard deviations of each region pair (denominator; representing local temporal variability). For the current relation between PCA dimensionality and local signal variability to be negative, it is necessary for the covariance between regions (the numerator term) to outpace the *SDx SDy* term (representing local temporal variability) in the denominator of the correlation formula. If the local variability of regions x and y was random noise, then the covariance between x and y should be minimized, pushing the correlation value to zero and the PCA dimensionality

estimate higher. In our results however, between-region correlations appear high (resulting in lower PCA dimensionality) *despite* high levels of local variability. As a simple demonstration that increasing randomness should invert the effect we find in our data, we simulated the impact of additive random noise on dimensionality by: (a) generating a matrix of in-phase sine waves (amplitude = 1) of equal spatiotemporal dimension to the original within-subject 2x2x2mm voxel-wise data (885*171922); (b) generating 171922 different vectors of uniformly distributed random noise (885*1) in varying proportions of the sine wave amplitude (here, 40 to 50%); (c) adding noise vectors to each generated sine wave (thus increasing total time series variation), and; (d) calculating PCA dimensionality of the entire spatiotemporal matrix at each noise level. In Figure S3, a clear positive (and effectively deterministic) linear effect between random noise level and PCA dimensionality emerges, the exact opposite effect we see in our data (see Figure 1).

On the other hand, influences that could drive the relation between local variability and network dimensionality in the observed negative direction is equally essential to consider. The most obvious fMRI artifact to account for in this regard is global signal (i.e., the average signal across the entire brain)[15]. Controversy remains regarding the nature of the global signal in fMRI, and whether or not it should be corrected[15,16]. Regardless of the mechanisms driving the global signal, this issue could be potentially salient for the present study given that by definition, a higher unifying between-region "global signal" would necessarily result in a lower dimensional spatiotemporal network organization. We thus computed the global signal within-subject (average of all voxels at each time point from a whole-brain mask (2mm standard MNI), yielding a single full-length time series), and regressed it from every voxel within-subject. From the global signal-regressed spatiotemporal matrix, we then recalculated PCA dimensionality and voxel-wise temporal variability within-person, and ran a new multivariate model linking the two. We first found that not only did PCA dimensionality values calculated from global signal regressed data correlate strongly with PCA dimensionality from non-regressed data (r = .86; bootstrap CI = .81, .91; $p = 4.68*10^{-31}$; Figure S4 (left)), but also that a very strong relation between network dimensionality and local temporal variability using global signal regressed data resulted (r = –.89; bootstrap CI = –.83, –.92; $p = 8.36*10^{-34}$; Figure S4 (right)). Global signal thus had little impact on our primary findings.

Network-specific models

Next, we examined whether pre-selection of *a priori* networks would affect the link between higher local temporal variability and lower network dimensionality. Most studies examining networks in fMRI data typically rely on network patterns resolved at the group level (e.g., using ICA[17-20]). Researchers' expectation of, or interest in, such group level networks (e.g., default mode network) may provide a clear rationale for network-specific probing of relations between PCA dimensionality and local variability. Employing a widely used, publicly-available 14-network parcellation[17], we re-computed (within-person) PCA dimensionality for each network independently; in this way, we estimated divergence from unidimensionality for each network separately, within-subject, and subsequently related that value directly to temporal variability only in network-specific voxels. For all networks, associations between local variability and network dimensionality were robustly negative, ranging from r = –.54 ($p = 8.31*10^{-9}$) to r = –.81 ($p = 3.39*10^{-24}$), with the strongest link again being expressed in the basal ganglia network (including thalamus, as in our overall model), as well as in the sensorimotor network (see Figures 2 and S5, and Table 1). To provide a complementary view on these network specific effects, we also calculated the variance accounted for by the first principal component (which necessarily accounts for the most within-subject spatiotemporal variance) from the within-subject PCA_{corr} solution for each network. Doing so provides an

alternative within-person measure of the divergence from spatial network unidimensionality (i.e., spatiotemporal divergence from the network template) that does not require setting an explicit summed variance criterion (e.g., 90%, as we have in the current study). First dimension variance accounted for correlated strongly with PCA dimensionality as estimated above (Figure S6), and as expected, correlated positively with local temporal variability (Figure S7 and Table S2). In the latter analysis, the effect sizes were somewhat reduced relative to those noted in Table 1, likely because of range truncation; first dimension variance, by definition, accounts for information contained only in the first dimension, whereas PCA dimensionality accounts for the vast majority of information contained in the entire spatiotemporal matrix. Regardless, these results suggest that the links we report between PCA dimensionality and local temporal variability above are not a function of arbitrary choice of threshold (i.e., 90% of total spatiotemporal data), but rather, represent a more general relation between divergence from network unidimensionality and local temporal variability.

Local temporal variability upregulates from thalamus to its cortical targets, and correlates negatively with network dimensionality

In our overall model, moment-to-moment variability in thalamus was a peak correlate of lower network dimensionality, in line with our hypotheses (see Figure 1). The thalamus indeed maintains projections to the entire cortex, and is thought to relay and/or modulate information flow throughout the entire brain[9,10]. Importantly, animal work indicates that visual cortex may inherit and then upregulate temporal variability explicitly from thalamic inputs[6,8,11]. We thus tested next whether thalamo-cortical upregulation of signal variability is present in humans within and beyond visual cortex, and whether such upregulation relates to network dimensionality. Utilizing the Horn et al. [21] thalamic atlas, which parcellates the thalamus via its structural connections to seven different cortical targets (see Methods), we calculated within-person upregulation of temporal variability from thalamus to cortex and its relations to network dimensionality by: (1) cortically masking each of the Shirer et al.[17] networks by intersecting each network with the Harvard-Oxford Cortical Atlas[23]; (2) manually determining which thalamic projections from the Horn et al. atlas are associated with the cortical regions within each subnetwork (see Figure 3); (3) calculating the median temporal variability for relevant thalamic regions and then from cortical voxels within each network; (4) calculating PCA dimensionality from network-specific cortical voxels, and; (5) modelling the relation between within-network dimensionality and upregulation of temporal variability from corresponding thalamic regions to within-network cortical regions (see Methods). We did not submit the basal ganglia network for further analysis as only 4% of its voxels were localized in cortical areas. All other networks (=13) were largely localized within the cortical regions displayed in the Harvard-Oxford atlas (82%–94% overlap), with a somewhat lower overlap for the right executive control network (67%) and the sensorimotor network (53%). Beyond evidence for *a priori* hypothesized upregulation is visual networks, we found significant upregulation in temporal variability from thalamus to cortical targets in all 13 examined networks (see Figure 3 and Table 2). This provides the first support in humans of animal work[6,8,11] suggesting upregulation of temporal variability from thalamus to cortex. Critically, we also found that in 12 out of 13 networks, greater within-person upregulation of temporal variability from thalamus to cortex coincided with lower within-network dimensionality (see Methods for model details, Table S3 for Q-Q plot outlier corrected models, and Table S4 for full sample results). These findings thus suggest that greater upregulation of local temporal variability from thalamus to cortex provides a key signature of how the brain communicates functionally overall.

Discussion

Our results demonstrate that high levels of temporal variability in regions of the human brain reflect lower functional network dimensionality regardless of adult age, specific power band, dimensionality estimation method, global signal regression, or regions/networks of interest. Our findings converge with recent computational and animal work suggesting that local variability may be largely generated directly from network interactions[24-26]. Local spiking variance (in area V1) is maximally shared among neurons that are similarly "tuned" (a hallmark of functional connectivity)[6,7]; beyond visual cortex however, we find that local variability reflects network dimensionality across the entire human brain. Perhaps most striking is the proportion of local dynamics accounted for by network dimensionality, ranging from correlations of $r = -.54$ to $-.81$ in individual networks, and $r = -.84$ at the whole brain level. It thus appears that local variability largely reflects the dimensionality of functional integration. Regarding how higher local variability could be produced from a lower dimensional functionally connected brain, computational and animal work suggests that greater moment-to-moment local variability may be driven by networks with balanced excitation and inhibition, particularly when connections are clustered or structured[26-30] (perhaps akin to our measure of network dimensionality). A key hallmark of balanced networks is that fluctuations in synaptic input (via network connectivity) reliably produce output fluctuations at the single cell level[26,31]. Because lower network dimensionality correlates with higher local variability in the current study, it is testable in future studies (e.g., via magnetic resonance spectroscopy) whether excitatory-inhibitory balance lies at the root of our findings. Although debate continues as to whether and how BOLD may capture inhibition, the on- and offset of excitation (glutamatergic release) likely captured by BOLD dynamics[32,33] may serve as an effective proxy to test for balanced networks.

Thalamic, and thalamo-cortical upregulation of, temporal variability and relations to network dimensionality

We also found that the thalamus was particularly salient correlate of network dimensionality in our overall model. Computational and animal work indeed suggests that the thalamus (lateral geniculate) may provide a primary source of local dynamics for visual cortex[34], suggesting the presence of network integration as a driver of local variability[35]; strikingly, our findings indicate that greater temporal variability in thalamus is also one of the strongest markers of lower dimensional functional connectivity in the human brain overall. Given that the thalamus maintains either afferent or efferent projections with most cortical regions[36-39], the thalamus may indeed serve as a putative hub[40] or generator of local dynamics throughout the human brain.

To better test the importance of the thalamus in the current context, we first sought to test *a priori* whether thalamo-cortical upregulation in variability was present in the current sample. Prior evidence for this effect existed only for studies of cat and macaque visual systems[6,8,11], with no published studies showing the reverse effect (i.e., reduction in variability from thalamus to cortex). We found first evidence in the current study not only for thalamo-cortical upregulation in visual networks in humans, but also that such upregulation may be a general property of human brain function independent of cortical (or network) target. Why should variability increase from thalamus to cortex? Goris et al.[8] offer the most convincing model-based account to date; they argue that fluctuations in neural gain (i.e., neural excitability) increase from thalamus to cortex, and are then a primary "source" of thalamo-cortical upregulation in variability overall. By reflecting neural excitability, the gain parameter represents modulatory influences on neural function, likely reflecting synaptic activity/potentiation. Further, fluctuations in gain may occur primarily on the order of minutes[8]. These two features permit the consideration of BOLD in relation to the Goris et al. model; BOLD is indeed most closely linked to synaptic (modulatory) activity[41], and can

easily approximate the time scale of gain fluctuations proposed. In particular, BOLD also likely dominantly reflects glutamatergic (excitatory) activity, rather than inhibitory sources; as such, fluctuations in BOLD may represent fluctuations in the excitatory system directly, thus approximating the Goris et al. view of variance in neural gain (excitability) as the primary feature of thalamo-cortical upregulation in variability. There are many potential influences on fluctuations in neural excitability that could be tested in future studies of moment-to-moment BOLD signal variability, such as attention/vigilance, system arousal/wakefulness, and reward[8]. One interesting and testable example prediction in future studies is that thalamo-cortical upregulation in variability should modulate with parametric changes in attentional load or sensory evidence.

Regarding why variability may be higher in cortex than in thalamus, Goris et al.[8] argue that the visual cortex is required to integrate a greater number of differing input sources (e.g., intra- and inter-cortically; thalamo-cortically; top-down inputs), which may all have their own modulatory influences at different temporal scales. Indeed, the sheer number of cortico-cortical connections far outweighs the number of thalamo-cortical connections[42-44]. Accordingly, higher cortical variability (which we generally find is indicative of optimal cognitive performance[2,12,45,46]) may be a direct reflection of a more complex process of "local" integration over differentiated inputs. Strikingly, we also found that greater thalamo-cortical upregulation in variability was a hallmark of lower network dimensionality in nearly all brain networks considered (the sensorimotor network also showed the same directionality of effect as all others, only under threshold), suggesting that thalamo-cortical upregulation may also provide a signature of generalized, distributed (as well as local) neural integration. Further, as another potential determinant of thalamo-cortical upregulation, observed temporal variance levels at the single cell level appear much more differentiated across cells in visual cortex compared to relatively homogeneous levels in thalamus[8]; given that fMRI captures ensemble level activity across millions of neurons per voxel, integrating spatially differentiated temporal variability levels across neurons into voxels could amount to a greater degree of ensemble-level temporal variance, compared to more spatially homogeneous voxels in thalamus. Thus, thalamo-cortical upregulation in BOLD variability could be a function of (1) increased need for functional integration over differing input types, and (2) heightened cell differentiation contributing to observed local (ensemble) dynamics, from thalamus to cortex.

Further comments

With regard to the potential functional relevance of the current resting-state results, past work suggests that greater local variability predicts faster and more stable reaction time performance, both within- and between- persons[2,12,45,47-49]; given that the present results demonstrate that higher local variability correlates strongly with lower network dimensionality, it is tempting to infer that relatively lower dimensionality may also serve as a marker of a well-functioning system on task. We contend, however, the optimal behavioral working point for level of network dimensionality will depend on experimental context. We do not propose that an optimal brain should approach uni-dimensionality (and presumably then, maximal local variability); it is rather more likely that the number of dimensions should be as low as is necessary given the contextual demands. Indeed, in the extreme, too-low dimensional neural systems may prove entirely dysfunctional (e.g., during epileptic seizure[50]). Future work using parametric task paradigms could more carefully address "optimal" network dimensionality levels associated with high cognitive performance.

Interestingly, recent work by Fusi and colleagues[51,52] highlights neuronal-based dimensionality from a complementary perspective. So-called "mixed selectivity neurons" (e.g., those that respond well to auditory *and* visual input) tend to exhibit higher "response"

dimensionality and thus permit system flexibility. However, highly selective neurons (e.g., those that respond only to visual input) are low dimensional by nature and may be useful when, for example, classification-type tasks are required (e.g., face/house discriminations[53,54]). In this way, higher and lower dimensionality may be beneficial under different constraints. Critically however, our current estimate of network dimensionality differs from this perspective in that it simply captures how brain regions are jointly coupled in time, regardless of whether neural ensembles respond to more or fewer stimulus types. Interestingly, because mixed selectivity neurons would by definition correlate with a greater number of different types of neurons, then if anything, network dimensionality would reduce in the presence of mixed selectivity neurons (e.g., such neurons would be more likely to statistically "cross-load" on to different networks, rather than exhibit unique properties), potentially also exhibiting greater signal variability at the local level, as our current findings would suggest. It remains an open question whether network dimensionality would respond differentially to cognitive contexts in which mixed selectivity and highly selective neurons may operate simultaneously (e.g., by ramping parametric task complexity, such as employing a parametric multisensory integration paradigm).

Conclusion

Using publicly available fMRI data, the current results provide for an immediately (re)testable, context-independent hypothesis in future work – that the degree of local, observed moment-to-moment variability primarily reflects the level of functional integration in the human brain, and that the thalamus may play a particularly important role in this effect.

Methods

Neuroimaging, preprocessing, and analyses

We utilized high-speed, multiband fMRI resting state data from 100 healthy adult participants (age range = 18–83 years) from the NKI-Enhanced dataset (publicly available at http://fcon_1000.projects.nitrc.org/indi/enhanced/download.html). All participants were reported to be psychiatrically and neurologically healthy, and had structural and functional neuroimages free of major artifacts upon initial screening. As noted in Nooner *et al.*[14], Institutional Review Board Approval was obtained for the NKI-Enhanced project at the Nathan Kline Institute (Phase I #226781 and Phase II #239708) and at Montclair State University (Phase I #000983A and Phase II #000983B). Written informed consent was obtained for all study participants.

Whole-brain resting-state fMRI data (10 mins, 900 volumes total) were collected via a 3T Siemens TrioTim MRI system (Erlangen, Germany) using a multi-band EPI sequence (TR = 645 ms; TE = 30 ms; flip angle 60°; FoV = 222 mm; voxel size 3x3x3 mm; 40 transverse slices; for full scanning protocol, see http://fcon_1000.projects.nitrc.org/indi/pro/eNKI_RS_TRT/__Rest_645.pdf). The first 15 volumes (15 × 645 ms = 9.7 sec) were removed to ensure a steady state of tissue magnetization (total remaining volumes = 885). A T1-weighted structural scan was also acquired to enable co-registration to functional images (MPRAGE: TR = 1900 ms; TE = 2.52 ms; flip angle 9°; FoV= 250 mm; voxel size 1x1x1 mm; 176 sagittal slices; full details at http://fcon_1000.projects.nitrc.org/indi/enhanced/NKI_MPRAGE.pdf).

fMRI data were preprocessed with FSL 5[55,56]. Pre-processing included motion-correction and bandpass filtering (.01–.10 Hz). We registered functional images to participant-specific T1 images, and from T1 to 2mm standard space (MNI 152_T1) using FLIRT. We then masked

the functional data with the GM tissue prior provided in FSL (thresholded at probability > 0.37). We detrended the data (up to a cubic trend) using the SPM_detrend function in SPM8. We also utilized extended preprocessing steps to further reduce data artifacts[45,46,57]. Specifically, we subsequently examined all functional volumes for artifacts via independent component analysis (ICA) within-run, within-person, as implemented in FSL/MELODIC[19]. Noise components were identified according to several key criteria: a) Spiking (components dominated by abrupt time series spikes); b) Motion (prominent edge or "ringing" effects, sometimes [but not always] accompanied by large time series spikes); c) Susceptibility and flow artifacts (prominent air-tissue boundary or sinus activation; typically represents cardio/respiratory effects); d) White matter (WM) and ventricle activation[58]; e) Low-frequency signal drift[59]; f) High power in high-frequency ranges unlikely to represent neural activity (≥ 75% of total spectral power present above .10 Hz;); and g) Spatial distribution ("spotty" or "speckled" spatial pattern that appears scattered randomly across ≥ 25% of the brain, with few if any clusters with ≥ 80 contiguous voxels [at 2x2x2 mm voxel size]). Examples of these various components we typically deem to be noise can be found in supplementary materials in Garrett et al.[12] By default, we utilized a conservative set of rejection criteria; if manual classification decisions were challenging due to mixing of "signal" and "noise" in a single component, we generally elected to keep such components. Three independent raters of noise components were utilized; > 90% inter-rater reliability was required on separate data before denoising decisions were made on the current data. Components identified as artifacts were then regressed from corresponding fMRI runs using the regfilt command in FSL.

Voxel-wise estimates of signal variability

Voxel-wise signal variability was calculated using the square root of power (summed between .01–.10 Hz) derived from the *pwelch* function in Matlab. This quantity is akin to the standard deviation of the time series within the same frequency range.

Network dimensionality estimation

Our primary within-subject network dimensionality estimation technique utilized "spatial" principal components analysis (PCA), which decomposes a correlation matrix (voxel_corrs) for all voxel pairs from each within-subject spatiotemporal matrix (885*171922),

$$\mathrm{PCA}_{(\mathrm{voxel_corrs})} = USV'$$

where U and V are the left and right eigenvectors, and S is a diagonal matrix of eigenvalues. We then counted the number of dimensions it took to capture 90% of the within-subject voxel correlation data. Because the S matrix represents the eigenvalues of the solution, and each eigenvalue is proportional to the variance accounted for in the entire decomposition, we summed eigenvalues until 90% of the total variance was reached. The fewer dimensions there are for a given subject, the more that voxels correlate with each other across time points. The same decomposition technique was also applied to 14 individual *a priori* network matrices reported and made publicly available by Shirer et al.[17]. We calculated a within-subject, between-voxel correlation matrix using only those voxels contained within each *a priori* network, and ran each network matrix through PCA to calculate a within-person, network-specific dimensionality score. In this way, we estimated individual differences in the dimensionality of previously defined, group-level networks. We chose to use the Shirer et al.[17] networks given the authors' inclusion of subcortical structures in the possible network space, unlike other commonly utilized, but cortical network-only, alternatives[60].

Statistical modeling: Partial Least Squares

To examine multivariate relations between PCA dimensionality and $BOLD_{power}$, we utilized a behavioural PLS analysis[61,62], which begins by calculating a between-subject correlation matrix (CORR) between (1) PCA dimensionality (PCA_{dim}) and (2) each voxel's $BOLD_{power}$ value. CORR is then decomposed using singular value decomposition (SVD).

$$SVD_{CORR\ (BOLDpower,\ PCAdim)} = USV'$$

This decomposition produces a left singular vector of PCA_{dim} weights (U), a right singular vector of brain voxel weights (V), and a diagonal matrix of singular values (S). A single estimable latent variable (LV) results that represents the relations between PCA dimensionality and $BOLD_{power}$ values. This LV contains a spatial activity pattern depicting the brain regions that show the strongest relation to network dimensionality identified by the LV. Each voxel weight (in V) is proportional to the voxel-wise correlation between voxel PCA_{dim} and $BOLD_{power}$.

Significance of detected relations was assessed using 1000 permutation tests of the singular value corresponding to the LV. A subsequent bootstrapping procedure revealed the robustness of within-LV voxel saliences across 1000 bootstrapped resamples of the data[63]. By dividing each voxel's weight (from V) by its bootstrapped standard error, we obtained "bootstrap ratios" (BSRs) as normalized estimates of robustness. For the whole brain analysis, we thresholded BSRs at values of ±3.00 (which exceeds a 99% confidence interval) and ±24.00 (see Figure 1). For the network-specific analyses, we threholded at ±3.00.

We also obtained a summary measure of each participant's robust expression of a particular LV's spatial pattern (a within-person "brain score") by multiplying the model-based vector of voxel weights (V) by each subject's vector of voxel $BOLD_{power}$ values (Q), producing a single within-subject value,

$$\text{Brain score} = VQ'$$

Brain scores are plotted on the y-axes of various models noted in Figures 1, 2, S1, S2, S4, and S7.

Statistical modeling of thalamo-cortical upregulation and its correlation to network dimensionality

We addressed the question whether thalamo-cortical upregulation of local signal variability is present in humans for 13 *a priori* networks from Shirer et al. [17]. We therefore manually determined the assignment of each of the network clusters to one or more of the seven cortical target areas suggested by Horn et al.[21], corresponding to the cortical lobes utilized in Behrens et al. [22] (we chose the Horn et al. atlas as a result of its derivation from an adult sample (N = 169) far larger than that utilized by Behrens et al.[22] (N = 7)). In this way we assigned one or more of the seven thalamic subdivisions to each Shirer et al. network (see Figure 3). Since we were only interested in projections from thalamus to cortex, all networks were cortically masked via the Harvard-Oxford Cortical Atlas using a probability threshold of 5% (Desikan, 2006) prior to analyses. As the basal-ganglia network only contained 4% cortical voxels, it was not considered further, and all successive analyses were calculated on the remaining 13 networks. Subsequently, for every subject and network, we calculated the median temporal variability of all cortical network voxels and all voxels within corresponding thalamic subdivisions. To test for significant within-subject thalamo-cortical upregulation, these median values were subjected to two-tailed, paired-sample t-tests for every network. To

model the relation between the upregulation of temporal variability to within-network dimensionality, we first re-calculated within-person, network-specific PCA dimensionality scores (as described above), although only using cortical voxels from each network within the PCA. The relation between thalamo-cortical upregulation of temporal variability and dimensionality was then formalized for each network by a multiple regression of the form

$$DIFF_{cortex-\ thalamus} = a + b_1\ VAR_{thalamus} + b_2\ PCA_{dim} + e$$

where $DIFF_{cortex-\ thalamus}$ is the difference score between cortical and thalamic temporal variability, $VAR_{thalamus}$ is the thalamic temporal variability and PCA_{dim} is the within-subject PCA dimensionality within cortical network regions. The partial regression coefficient b_2 quantifies the relation between the PCA dimensionality and thalamo-cortical difference in variability ('upregulation'), while controlling for baseline (i.e., thalamic) variability (see Table S5). All models were multivariate outlier-corrected, discarding the worst 5% within a Q-Q plot displaying the Mahalanobis distance (chi-squared distribution, *df* = 2) per network model. The Mahalanobis distance is a multi-dimensional measure of the distance of each point to the centroid of the (in our case, multivariate) distribution[64]. To gauge the effect of not accounting for outliers, we also include full sample statistics in Table S6.

Publicly available data and code

All data are already publicly available at http://fcon_1000.projects.nitrc.org/indi/enhanced/download.html. We will make our subject ID list, rationale for sample selection, and all code written to reproduce the current results, available upon request.

Acknowledgments

D.D.G was supported by an Emmy Nöther Programme grant from the German Research Foundation. U.L. acknowledges financial support from the Intramural Innovation Fund of the Max Planck Society. D.D.G and U.L. were also partially supported by the Max Planck UCL Centre for Computational Psychiatry and Ageing Research. Finally, we would like to thank Steffen Wiegert for assistance with data processing, and Andreas Brandmaier, Julian Kociessa, and Nathan Spreng for helpful discussions throughout the project.

References

1. Faisal, A. A., Selen, L. P. J. & Wolpert, D. M. Noise in the nervous system. *Nat Rev Neurosci* **9,** 292–303 (2008).
2. Garrett, D. D. *et al.* Moment-to-moment brain signal variability: A next frontier in human brain mapping? *Neuroscience & Biobehavioral Reviews* **37,** 610–624 (2013).
3. Shadlen, M. N. & Newsome, W. T. The variable discharge of cortical neurons: implications for connectivity, computation, and information coding. *J. Neurosci.* **18,** 3870–3896 (1998).
4. Mišić, B., Vakorin, V. A., Paus, T. & McIntosh, A. R. Functional embedding predicts the variability of neural activity. *Front. Sys. Neurosci.* **5,** (2011).
5. Pincus, S. M. Greater signal regularity may indicate increased system isolation. *Mathematical Biosciences* **122,** 161–181 (1994).
6. Scholvinck, M. L., Saleem, A. B., Benucci, A., Harris, K. D. & Carandini, M. Cortical State Determines Global Variability and Correlations in Visual Cortex. *J. Neurosci.* **35,** 170–178 (2015).
7. Lin, I.-C., Okun, M., Carandini, M. & Harris, K. D. The Nature of Shared Cortical Variability. *Neuron* **87,** 644–656 (2015).
8. Goris, R. L. T., Movshon, J. A. & Simoncelli, E. P. Partitioning neuronal variability. *Nature Neuroscience* **17,** 858–865 (2014).
9. Bell, P. T. & Shine, J. M. Subcortical contributions to large-scale network communication. *Neuroscience & Biobehavioral Reviews* **71,** 313–322 (2016).
10. Sherman, S. M. Thalamus plays a central role in ongoing cortical functioning. *Nat Neur* **19,** 533–541 (2016).
11. Kara, P., Reinagel, P. & Reid, R. C. Low Response Variability in Simultaneously Recorded Retinal, Thalamic, and Cortical Neurons. *Neuron* **27,** 635–646 (2000).
12. Garrett, D., McIntosh, A. R. & Grady, C. L. Brain Signal Variability is Parametrically Modifiable. *Cereb. Cortex* **24,** 2931–2940 (2014).
13. Garrett, D., Kovacevic, N., McIntosh, A. R. & Grady, C. L. The Modulation of BOLD Variability between Cognitive States Varies by Age and Processing Speed. *Cereb. Cortex* **23,** 684–693 (2013).
14. Nooner, K. B. *et al.* The NKI-Rockland Sample: A Model for Accelerating the Pace of Discovery Science in Psychiatry. *Front. Neurosci.* **6,** 152 (2012).
15. Liu, T. T., Nalci, A. & Falahpour, M. The global signal in fMRI: Nuisance or Information? *NeuroImage* **150,** 213–229 (2017).
16. Power, J. D., Plitt, M., Laumann, T. O. & Martin, A. Sources and implications of whole-brain fMRI signals in humans. *NeuroImage* **146,** 609–625 (2017).
17. Shirer, W. R., Ryali, S., Rykhlevskaia, E., Menon, V. & Greicius, M. D. Decoding Subject-Driven Cognitive States with Whole-Brain Connectivity Patterns. *Cereb. Cortex* **22,** 158–165 (2011).
18. Damoiseaux, J. S. *et al.* Consistent resting-state networks across healthy subjects. *Proc. Natl. Acad. Sci. U.S.A.* **103,** 13848–13853 (2006).
19. Beckmann, C. F. & Smith, S. M. Probabilistic Independent Component Analysis for Functional Magnetic Resonance Imaging. *IEEE Trans Med Imaging* **23,** 137–152 (2004).
20. Salami, A., Pudas, S. & Nyberg, L. Elevated hippocampal resting-state connectivity underlies deficient neurocognitive function in aging. *Proc. Natl. Acad. Sci. U.S.A.* **111,** 17654–17659 (2014).
21. Horn, A. & Blankenburg, F. Toward a standardized structural–functional group connectome in MNI space. *NeuroImage* **124,** 310–322 (2016).
22. Behrens, T. E. J. *et al.* Non-invasive mapping of connections between human thalamus

and cortex using diffusion imaging. *Nature Neuroscience* **6,** 750–757 (2003).
23. Desikan, R. S. *et al.* An automated labeling system for subdividing the human cerebral cortex on MRI scans into gyral based regions of interest. *NeuroImage* **31,** 968–980 (2006).
24. Van Vreeswijk, C. & Sompolinsky, H. Chaos in neuronal networks with balanced excitatory and inhibitory activity. *Science* **274,** 1724–1726 (1996).
25. Van Vreeswijk, C. & Sompolinsky, H. Chaotic balanced state in a model of cortical circuits. *Neural Comput* **10,** 1321–1371 (1998).
26. Doiron, B. & Litwin-Kumar, A. Balanced neural architecture and the idling brain. *Front. Comput. Neurosci.* **8,** 237 (2014).
27. Doiron, B., Litwin-Kumar, A., Rosenbaum, R., Ocker, G. K. & Josic, K. The mechanics of state-dependent neural correlations. *Nature Neuroscience* **19,** 383–393 (2016).
28. Litwin-Kumar, A. & Doiron, B. Slow dynamics and high variability in balanced cortical networks with clustered connections. *Nature Neuroscience* **15,** 1498–1505 (2012).
29. Shew, W. L., Yang, H., Yu, S., Roy, R. & Plenz, D. Information Capacity and Transmission Are Maximized in Balanced Cortical Networks with Neuronal Avalanches. *J. Neurosci.* **31,** 55–63 (2011).
30. Shew, W. L., Yang, H., Petermann, T., Roy, R. & Plenz, D. Neuronal Avalanches Imply Maximum Dynamic Range in Cortical Networks at Criticality. *J. Neurosci.* **29,** 15595–15600 (2009).
31. Shadlen, M. N. & Newsome, W. T. Noise, neural codes and cortical organization. *Current Opinion in Neurobiology* **4,** 569–579 (1994).
32. Logothetis, N. K. What we can do and what we cannot do with fMRI. *Nature* **453,** 869–878 (2008).
33. Bojak, I., Oostendorp, T. F., Reid, A. T. & Kotter, R. Connecting Mean Field Models of Neural Activity to EEG and fMRI Data. *Brain Topogr* **23,** 139–149 (2010).
34. Sadagopan, S. & Ferster, D. Feedforward Origins of Response Variability Underlying Contrast Invariant Orientation Tuning in Cat Visual Cortex. *Neuron* **74,** 911–923 (2012).
35. Wang, H. P., Spencer, D., Fellous, J. M. & Sejnowski, T. J. Synchrony of Thalamocortical Inputs Maximizes Cortical Reliability. *Science* **328,** 106–109 (2010).
36. Lenglet, C. *et al.* Comprehensive in vivo Mapping of the Human Basal Ganglia and Thalamic Connectome in Individuals Using 7T MRI. *PLoS ONE* **7,** e29153 (2012).
37. Draganski, B. *et al.* Evidence for segregated and integrative connectivity patterns in the human Basal Ganglia. *J. Neurosci.* **28,** 7143–7152 (2008).
38. Ji, B. *et al.* Dynamic thalamus parcellation from resting-state fMRI data. *Hum. Brain Mapp.* **37,** 954–967 (2016).
39. Zhang, D. *et al.* Intrinsic Functional Relations Between Human Cerebral Cortex and Thalamus. *J Neurophysiol* **100,** 1740–1748 (2008).
40. Hwang, K., Bertolero, M., Liu, W. & D'Esposito, M. The human thalamus is an integrative hub for functional brain networks. *J. Neurosci.* **37,** 0067–17–5607 (2017).
41. Viswanathan, A. & Freeman, R. D. Neurometabolic coupling in cerebral cortex reflects synaptic more than spiking activity. *Nature Neuroscience* **10,** 1308–1312 (2007).
42. Latawiec, D., Martin, K. & Meskenaite, V. Termination of the geniculocortical projection in the striate cortex of macaque monkey: A quantitative immunoelectron microscopic study. *J. Comp. Neurol.* **419,** 306–319 (2000).
43. Binzegger, T., Douglas, R. J. & Martin, K. A quantitative map of the circuit of cat primary visual cortex. *J. Neurosci.* **24,** 8441–8453 (2004).
44. Douglas, R. J. & Martin, K. Neuronal circuits of the neocortex. *Annu. Rev. Neurosci.*

27, 419–451 (2004).
45. Garrett, D. D. *et al.* Amphetamine modulates brain signal variability and working memory in younger and older adults. *Proc. Natl. Acad. Sci. U.S.A.* **112,** 7593–7598 (2015).
46. Garrett, D., Kovacevic, N., McIntosh, A. R. & Grady, C. L. The Importance of Being Variable. *J. Neurosci.* **31,** 4496–4503 (2011).
47. Garrett, D. D., McIntosh, A. R. & Grady, C. L. Moment-to-moment signal variability in the human brain can inform models of stochastic facilitation now. *Nat Rev Neurosci* **12,** 612–612 (2011).
48. McIntosh, A. R., Kovacevic, N. & Itier, R. J. Increased brain signal variability accompanies lower behavioral variability in development. *PLoS Comput. Biol.* **4,** e1000106 (2008).
49. Misic, B., Mills, T., Taylor, M. J. & McIntosh, A. R. Brain Noise Is Task Dependent and Region Specific. *J Neurophysiol* **104,** 2667–2676 (2010).
50. Babloyantz, A. & Destexhe, A. Low-dimensional chaos in an instance of epilepsy. *Proc. Natl. Acad. Sci. U.S.A.* **83,** 3513–3517 (1986).
51. Fusi, S., Miller, E. K. & Rigotti, M. Why neurons mix: high dimensionality for higher cognition. *Current Opinion in Neurobiology* **37,** 66–74 (2016).
52. Rigotti, M. *et al.* The importance of mixed selectivity in complex cognitive tasks. *Nature* **497,** 585–590 (2013).
53. Park, J., Carp, J., Hebrank, A., Park, D. C. & Polk, T. A. Neural Specificity Predicts Fluid Processing Ability in Older Adults. *J. Neurosci.* **30,** 9253–9259 (2010).
54. Park, J. *et al.* Neural Broadening or Neural Attenuation? Investigating Age-Related Dedifferentiation in the Face Network in a Large Lifespan Sample. *J. Neurosci.* **32,** 2154–2158 (2012).
55. Smith, S. M. *et al.* Advances in functional and structural MR image analysis and implementation as FSL. *NeuroImage* **23,** S208–S219 (2004).
56. Jenkinson, M., Beckmann, C. F., Behrens, T. E. J., Woolrich, M. W. & Smith, S. M. FSL. *NeuroImage* **62,** 782–790 (2012).
57. Garrett, D., Kovacevic, N., McIntosh, A. R. & Grady, C. L. Blood Oxygen Level-Dependent Signal Variability Is More than Just Noise. *J. Neurosci.* **30,** 4914–4921 (2010).
58. Birn, R. M. The role of physiological noise in resting-state functional connectivity. *NeuroImage* **62,** 864–870 (2012).
59. Smith, A. M. *et al.* Investigation of Low Frequency Drift in fMRI Signal. *NeuroImage* **9,** 526–533 (1999).
60. Thomas Yeo, B. T. *et al.* The organization of the human cerebral cortex estimated by intrinsic functional connectivity. *J Neurophysiol* **106,** 1125–1165 (2011).
61. McIntosh, A. R., Bookstein, F. L., Haxby, J. V. & Grady, C. L. Spatial Pattern Analysis of Functional Brain Images Using Partial Least Squares. *NeuroImage* **3,** 143–157 (1996).
62. Krishnan, A., Williams, L. J., McIntosh, A. R. & Abdi, H. Partial Least Squares (PLS) methods for neuroimaging: A tutorial and review. *NeuroImage* **56,** 455–475 (2011).
63. Efron, B. & Tibshirani, R. *An introduction to the bootstrap.* (Chapman & Hall/CRC, 1993).
64. Mahalanobis, P. C. On the generalised distance in statistics. *Proceedings of the National Institute of Sciences of India, 1936* 49–55 (1936).

Tables

Table 1: Correlations between network-specific PCA dimensionality and network-voxel-specific local variability

Network	*r*	95% bootstrap CI	*p*
Anterior salience	-0.73	(-.66, -.81)	**$4.23*10^{-18}$**
Auditory	-0.72	(-.64, -.80)	**$2.76*10^{-17}$**
Basal ganglia	-0.81	(-.76, -.86)	**$3.39*10^{-24}$**
DMN (dorsal)	-0.75	(-.69, -.83)	**$1.78*10^{-19}$**
DMN (ventral)	-0.67	(-.59, -.75)	**$1.56*10^{-14}$**
Executive control (left)	-0.61	(-.50, -.71)	**$1.05*10^{-11}$**
Executive control (right)	-0.64	(-.56, -.72)	**$8.61*10^{-13}$**
High visual	-0.54	(-.46, -.64)	**$8.32*10^{-09}$**
Language	-0.68	(-.58, -.77)	**$4.94*10^{-15}$**
Posterior salience	-0.69	(-.60, -.77)	**$1.98*10^{-15}$**
Precuneus	-0.54	(-.40, -.65)	**$8.09*10^{-09}$**
Primary visual	-0.66	(-.59, -.74)	**$1.02*10^{-13}$**
Sensorimotor	-0.80	(-.75, -.85)	**$2.02*10^{-23}$**
Visuospatial	-0.68	(-.59, -.76)	**$1.21*10^{-14}$**

Note: Statistics represent network-specific PLS model runs for each network. 95% Bootstrap CI was computed via 1000 resamples with replacement of the data. Significant *p*-values are in bold font.

Table 2: Paired-sample *t*-tests comparing the median values of cortical and thalamic variability across subjects per network

Networks	Mean difference	Bootstrap 95% CI	SE	*t*	*p*
Auditory	172.44	(134.57, 210.31)	19.09	9.03	**$1.39*10^{-14}$**
DMN (dorsal)	262.29	(237.61, 286.97)	12.44	21.09	**$2.15*10^{-38}$**
DMN (ventral)	202.52	(180.52, 224.52)	11.09	18.27	**$1.77*10^{-33}$**
Executive control (left)	311.41	(282.96, 339.86)	14.34	21.72	**$1.92*10^{-39}$**
Executive control (right)	178.96	(155.22, 202.71)	11.97	14.95	**$3.83*10^{-27}$**
High visual	369.48	(317.09, 421.87)	26.40	13.99	**$3.39*10^{-25}$**
Language	118.74	(96.30, 141.18)	11.31	10.50	**$8.97*10^{-18}$**
Precuneus	443.85	(402.39, 485.31)	20.89	21.24	**$1.18*10^{-38}$**
Primary visual	385.89	(331.10, 440.68)	27.61	13.98	**$3.70*10^{-25}$**
Salience (anterior)	202.40	(175.28, 229.53)	13.67	14.81	**$7.57*10^{-27}$**
Salience (posterior)	199.03	(174.98, 223.08)	12.12	16.42	**$5.08*10^{-30}$**
Sensorimotor	26.35	(13.43, 39.26)	6.51	4.05	**$1.03*10^{-04}$**
Visuospatial	210.37	(187.30, 233.44)	11.63	18.09	**$3.73*10^{-33}$**

Note: SE = standard error. CI = confidence interval. *df* = 99 for all models.
Significant *p*-values are in bold font.

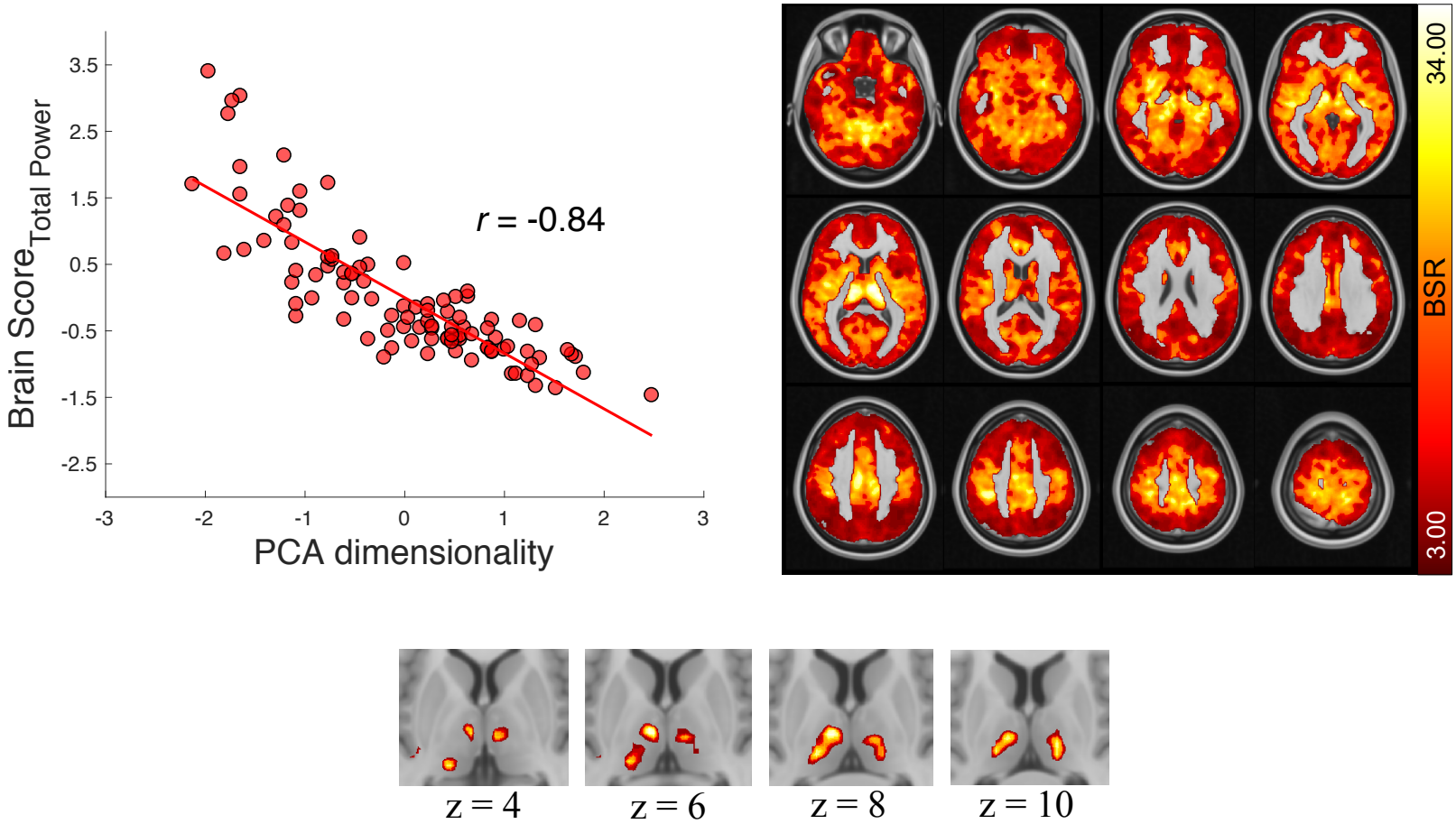

Figure 1: Network dimensionality negatively correlates with local temporal variability. Brain Score$_{\text{Total Power}}$ = PLS model-derived latent score representing local temporal variability (estimated by $\sqrt{power}$); BSR = bootstrap ratio (see Online Methods). Both axis variables are z-transformed. Top right: axial slices shown every 8mm from -24 to 64. Bottom row: due to global nature of the model effect at a typical threshold level (upper right panel), the bottom panel depicts the strongest spatial representations of the effect (bilateral thalamus; BSR = 24; peak MNI coordinates at [-8 -12 6] (183 voxels) and [14 -18 10], 155 voxels).

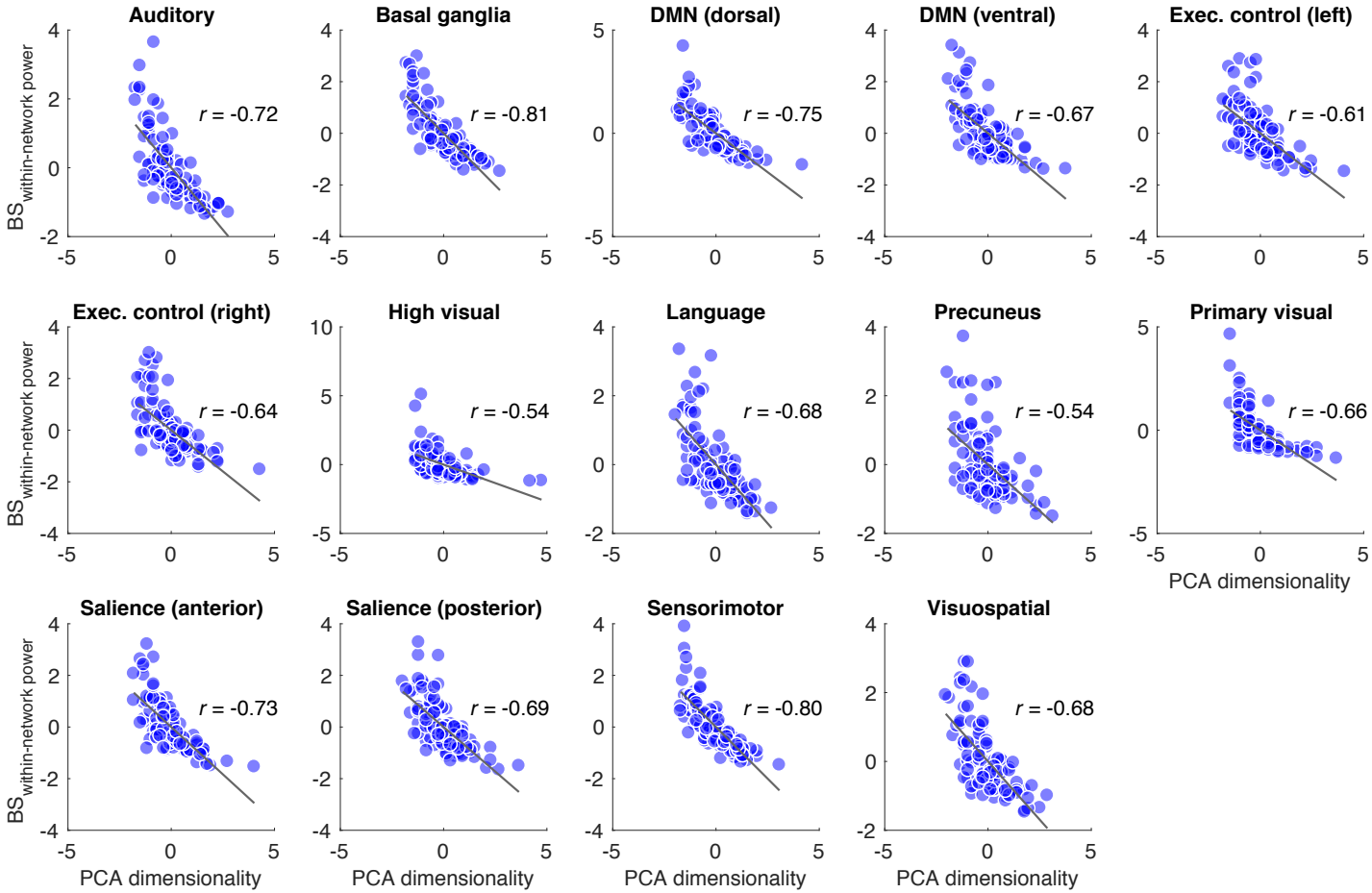

Figure 2: Consistent negative correlations between network dimensionality and local signal variability across possible a priori networks of interest. Network-specific PLS model runs. $BS_{\text{Within-Network Power}}$ = PLS model-derived latent brain score representing local temporal variability (estimated by $\sqrt{power}$). All axis variables are z-transformed. DMN = default mode network. High Visual network: when holding out the four most extreme outliers (two on x-axis and two on the y-axis), the correlation remains similar (r = -.60). Note the differences in value ranges on x and y axes across plots, which reflect differential within-network model fit.

A

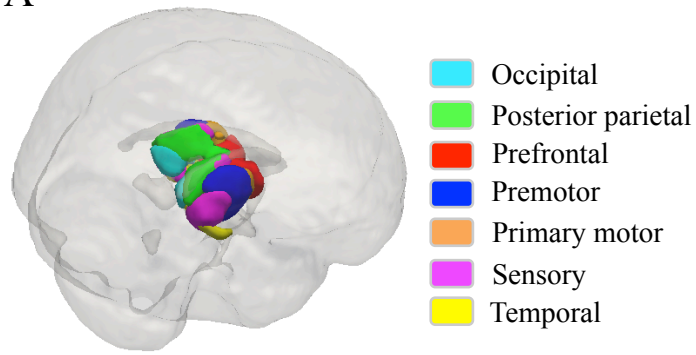

B

Shirer et al. networks	Occipital	Posterior parietal	Prefrontal	Premotor	Primary motor	Sensory	Temporal
	Horn et al thalamic regions						
Auditory			X				X
DMN (dorsal)		X	X				X
DMN (ventral)	X	X	X				X
Exec. control (left)		X	X				X
Exec. control (right)		X	X				
High visual	X						
Language		X	X				
Precuneus	X	X					
Primary visual	X						
Salience (anterior)			X	X			X
Salience (posterior)		X	X			X	X
Sensorimotor				X	X	X	
Visuospatial	X	X	X			X	X

C

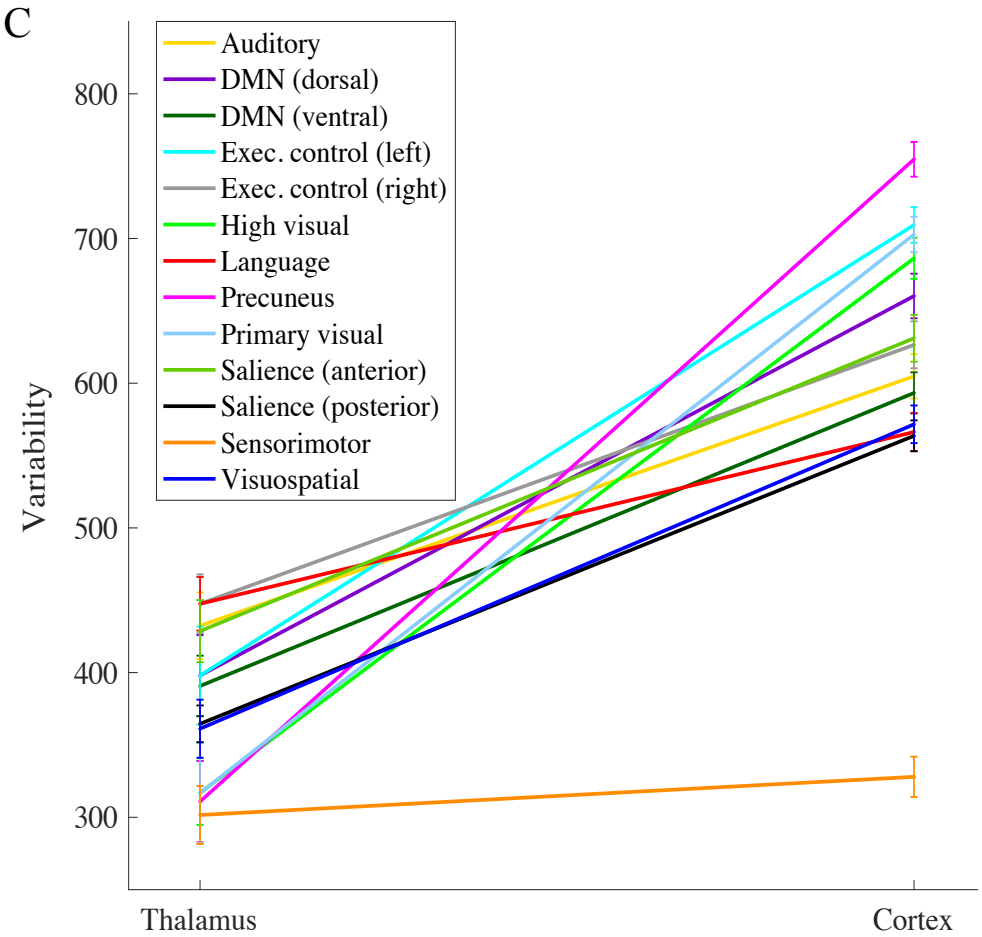

Figure 3: Within-network thalamo-cortical projection and upregulation. (A) Thalamic regions as in Horn et al.[21]. (B) Mapping of the thalamic regions to the Shirer et al.[17] networks. (C) Upregulation in local variability from Horn et al.[21] thalamic regions to cortical regions for each Shirer et al.[17] network. Values represent group averaged median thalamic and cortical variability levels, and error bars represent standard error of the mean across subjects.

Supplemental Information (SI)

Results

Control analyses for whole-brain model linking local temporal variability and network dimensionality

We subsequently probed the relation between within-voxel temporal variability and network dimensionality in multiple ways. First, given that much of our previous work has demonstrated that older adults express less temporal variability in brain signals[13,45,46,57], we examined whether the link between local variability and network dimensionality would hold after controlling for adult age. We found that network dimensionality strongly predicted local variability independent of age (semi-partial $r = -.74$). In line with our previous findings[13,45,46,57], local variability also decreased with age (see Table S1), although the zero-order effect of age ($r = -.46$) was somewhat attenuated (semi-partial $r = -.24$) when controlling for network dimensionality.

Second, for PCA dimensionality estimation in our primary results above, we decomposed a spatiotemporal correlation matrix (PCA_{corr}) as opposed to the more typical decomposition of a covariance matrix (see Methods). PCA is variance-sensitive by design, so decomposing a covariance matrix in which temporal variance is not scaled (as in PCA_{corr}) could bias the relation between local variability and PCA dimensionality. Conversely, decomposing a correlation matrix ensures that differential temporal variances between region pairs are accounted for (i.e., in the denominator of the correlation formula; see Methods for a description). In any case, our results showed that the relation between local variability ($\sqrt{power}$) and PCA_{corr} dimensionality (Figure 1) held in the absence of "variance bias." However, because other decomposition methods (i.e., covariance matrix-based PCA (PCA_{covar}) and independent components analysis (ICA, which seeks statistical independence between dimensions rather than orthogonality) are not only typical but also differ in potentially relevant ways from PCA_{corr}, we also investigated whether these alternative methods would grossly alter the relation between network dimensionality and local temporal variability. PCA_{covar} was run in the same manner as described in Methods, although using a within-subject, between-voxel covariance matrix instead of a correlation matrix. ICA was run via MELODIC in FSL[19]. In all cases, we counted how many dimensions were required to capture 90% of the spatiotemporal data, within-subject. Results indicated that PCA_{covar} ($r = .88$, bootstrap CI = -.84, -.91; $p = 2.58*10^{-33}$) and ICA ($r = .82$, bootstrap CI = -.72, -.90; $p = 1.67*10^{-25}$) dimensionality correlated strongly with PCA_{corr} dimensionality (see Figure 2, upper row). Separate PLS models were also robust (see Figure S1, lower row) when linking PCA_{covar} dimensionality to local variability ($r = -.66$, bootstrap CI = -.61, -.73; $p = 7.37*10^{-14}$) and ICA dimensionality to local variability ($r = -.64$, bootstrap CI = -.50, -.76; $p = 8.86*10^{-13}$). Thus, regardless of exact dimensionality estimation method, all results converged to demonstrate a reliable negative relation between network dimensionality and local temporal dynamics.

Third, because our primary results in the current paper gauge local temporal variability by estimating power in a typical bandpass range for fMRI (.01-.10 Hz), we also examined whether frequency range may influence the relation between PCA dimensionality and local voxel-wise variability. We separated the bandpass frequency range (.01-.10 Hz) into equal thirds (low, medium, high), calculated $\sqrt{power}$ for each voxel and frequency range (as our

estimate of local temporal variability), and then ran a PLS model linking PCA dimensionality to local variability for each frequency range. We found a single significant latent variable ($p = 1.08*10^{-27}$) demonstrating a similar effect as seen in our overall results; for low ($r = -.81$; 95% bootstrap CI = .76, .87), medium ($r = -.74$; 95% bootstrap CI = .69, .81), and high frequency ranges ($r = .71$; 95% bootstrap CI = .65, .78), network dimensionality and local variability were negatively correlated (see Figure S2).

Tables

Table S1: Regression model predicting PLS-derived, latent level, voxel-wise temporal variability

Predictor	*b*	Bootstrap 95% CI	SE	*t*	*p*	Zero-order	Partial	Semi-Partial	VIF
PCA dimensionality	-2532.81	(-2816.69, -2280.53)	167.19	-15.15	**$2.02*10^{-27}$**	-0.84	-0.84	-0.74	1.08
Adult age	-1034.77	(-1257.89, -794.25)	215.21	-4.81	**$6.00*10^{-6}$**	-0.46	-0.44	-0.24	1.08

Note: PCA = principal component analysis; CI = confidence interval; SE = standard error; VIF = variance inflation factor. Significant *p*-values are in bold font. 95% Bootstrap CI was computed via 1000 resamples with replacement of the data. “Zero-order”, “partial,” and “semi-partial” columns reflect effect sizes in Pearson’s correlation metric.

Table S2: Correlations between (a) variance accounted for by the first within-network PCA dimension and (b) network-voxel-specific local variability

Network	*r*	95% bootstrap CI	*p*
Auditory	.65	(.54, .75)	**$2.17*10^{-13}$**
Basal ganglia	.67	(.55, .77)	**$1.66*10^{-14}$**
DMN (dorsal)	.47	(.32, .62)	**$8.72*10^{-7}$**
DMN (ventral)	.56	(.38, .70)	**$1.73*10^{-9}$**
Executive control (left)	.35	(.14, .54)	**$4.47*10^{-4}$**
Executive control (right)	.33	(.13, .50)	**$8.35*10^{-4}$**
High visual	.36	(.20, .52)	**$2.06*10^{-4}$**
Language	.55	(.38, .69)	**$2.77*10^{-9}$**
Precuneus	.49	(.33, .62)	**$2.58*10^{-7}$**
Primary visual	.60	(.49, .69)	**$4.88*10^{-11}$**
Salience (anterior)	.54	(.40, .65)	**$9.84*10^{-9}$**
Salience (posterior)	.40	(.21, .57)	**$4.60*10^{-5}$**
Sensorimotor	.55	(.40, .67)	**$3.73*10^{-9}$**
Visuospatial	.55	(.41, .67)	**$3.24*10^{-9}$**

.

Table S3: Regression model predicting thalamo-cortical variability upregulation from dimensionality and controlled for by thalamic variability, outlier-corrected (N=95 for every model)

Dependent variable: Power difference (within-network)	Predictor	*b*	Bootstrap 95% CI	SE	*t*	*p*	Zero-order	Part	Partial	VIF
Auditory	Thalamic variability	0.10	(-0.29, 0.52)	0.15	0.70	0.49	0.42	0.07	0.06	1.57
	PCA dimensionality	-28.15	(-41.15, -16.43)	5.01	-5.62	**$2.05*10^{-7}$**	-0.62	-0.51	-0.46	1.57
DMN (dorsal)	Thalamic variability	-0.38	(-0.63, -0.13)	0.11	-3.35	**$1.12*10^{-3}$**	0.12	-0.33	-0.29	1.76
	PCA dimensionality	-18.16	(-23.70, -12.72)	2.72	-6.68	**$1.83*10^{-9}$**	-0.50	-0.57	-0.57	1.76
DMN (ventral)	Thalamic variability	-0.15	(-0.44, 0.16)	0.12	-1.19	0.24	0.12	-0.12	-0.12	1.72
	PCA dimensionality	-9.43	(-14.18, -3.98)	2.86	-3.30	**$1.39*10^{-3}$**	-0.32	-0.33	-0.32	1.72
Exec. control (left)	Thalamic variability	-0.06	(-0.34, 0.24)	0.13	-0.42	0.68	0.20	-0.04	-0.04	1.37
	PCA dimensionality	-21.91	(-29.64, -14.36)	4.98	-4.40	**$2.90*10^{-5}$**	-0.45	-0.42	-0.41	1.37
Exec. control (right)	Thalamic variability	0.03	(-0.16, 0.20)	0.10	0.31	0.76	0.16	0.03	0.03	1.19
	PCA dimensionality	-12.64	(-19.47, -5.78)	4.36	-2.90	**$5.0*10^{-3}$**	-0.33	-0.29	-0.29	1.19
High visual	Thalamic variability	0.43	(-0.18, 1.10)	0.24	1.84	0.07	0.35	0.19	0.16	1.16
	PCA dimensionality	-42.49	(-58.13, -27.87)	8.50	-5.00	**$3.0*10^{-6}$**	-0.53	-0.46	-0.43	1.16
Language	Thalamic variability	-0.15	(-0.35, 0.04)	0.10	-1.50	0.14	0.10	-0.15	-0.15	1.64
	PCA dimensionality	-11.36	(-16.05, -6.43)	3.12	-3.65	**$4.42*10^{-4}$**	-0.34	-0.36	-0.35	1.64
Precuneus	Thalamic variability	0.41	(-0.14, 0.95)	0.22	1.85	0.07	0.32	0.19	0.17	1.18
	PCA dimensionality	-28.79	(-45.85, -12.96)	8.96	-3.21	**$2.0*10^{-3}$**	-0.40	-0.32	-0.30	1.18
Primary visual	Thalamic variability	0.51	(-0.08, 1.20)	0.26	1.97	0.05	0.40	0.20	0.16	1.25
	PCA dimensionality	-74.91	(-100.06, -55.26)	14.06	-5.33	**$6.73*10^{-7}$**	-0.57	-0.48	-0.44	1.25
Salience (anterior)	Thalamic variability	-0.04	(-0.32, 0.20)	0.12	-0.35	0.72	0.32	-0.04	-0.03	1.70
	PCA dimensionality	-15.06	(-21.43, -9.65)	3.12	-4.83	**$5.0*10^{-6}$**	-0.53	-0.45	-0.43	1.70
Salience (posterior)	Thalamic variability	0.02	(-0.31, 0.35)	0.13	0.18	0.86	0.22	0.02	0.02	1.45
	PCA dimensionality	-12.91	(-18.95, -6.30)	4.29	-3.01	**$3.0*10^{-3}$**	-0.36	-0.30	-0.29	1.45
Sensorimotor	Thalamic variability	-0.11	(-0.36, 0.23)	0.10	-1.13	0.26	-0.03	-0.12	-0.12	1.49
	PCA dimensionality	-2.78	(-6.23, 0.81)	1.73	-1.61	0.11	-0.12	-0.17	-0.17	1.49
Visuospatial	Thalamic variability	0.00	(-0.31, 0.32)	0.13	0.03	0.98	0.28	0.00	0.00	1.63
	PCA dimensionality	-10.42	(-15.70, -5.43)	2.76	-3.78	**$2.83*10^{-4}$**	-0.45	-0.37	-0.35	1.63

Note: Power difference = within-network cortical variability minus thalamic variability (estimated by $\sqrt{power}$). PCA = principal component analysis; CI = confidence interval; SE = standard error; VIF = variance inflation factor. Significant *p*-values are in bold font. 95% Bootstrap CI was computed via 1000 resamples with replacement of the data. "Zero-order", "partial," and "semi-partial" columns reflect effect sizes in Pearson's correlation metric.

Table S4: Regression model predicting thalamo-cortical variability upregulation from dimensionality and controlled for by thalamic variability, N=100

Dependent variable: Thalamo-cortical variability difference (within-network)	Predictor	*b*	Bootstrap 95% CI	SE	*t*	*p*	Zero-order	Part	Partial	VIF
Auditory	Thalamic variability	-0.08	(-0.35, 0.29)	0.13	-0.67	0.51	0.30	-0.07	-0.06	1.54
	PCA dimensionality	-28.90	(-18.53, -18.53)	4.67	-6.18	**$1.48*10^{-8}$**	-0.59	-0.53	-0.51	1.54
DMN (dorsal)	Thalamic variability	-0.14	(-0.42, 0.14)	0.10	-1.37	0.18	0.23	-0.14	-0.12	1.72
	PCA dimensionality	-13.99	(-20.20, -8.90)	2.65	-5.28	**$8.08*10^{-7}$**	-0.50	-0.47	-0.46	1.72
DMN (ventral)	Thalamic variability	0.04	(-0.23, 0.21)	0.10	0.36	0.72	0.28	0.04	0.03	1.76
	PCA dimensionality	-7.46	(-11.93, -3.17)	2.61	-2.86	**$5.13*10^{-3}$**	-0.39	-0.28	-0.27	1.76
Exec. control (left)	Thalamic variability	-0.01	(-0.28, 0.26)	0.11	-0.07	0.95	0.21	-0.01	-0.01	1.31
	PCA dimensionality	-19.36	(-26.92, -12.28)	4.68	-4.14	**$7.50*10^{-5}$**	-0.43	-0.39	-0.38	1.31
Exec. control (right)	Thalamic variability	0.01	(-0.15, 0.16)	0.08	0.13	0.90	0.14	0.01	0.01	1.23
	PCA dimensionality	-10.70	(-17.19, -5.06)	3.93	-2.72	**$7.6*10^{-3}$**	-0.30	-0.27	-0.26	1.23
High visual	Thalamic variability	0.68	(0.11, 1.19)	0.19	3.58	**$5.42*10^{-4}$**	0.47	0.34	0.29	1.17
	PCA dimensionality	-30.25	(-48.53, -19.17)	6.73	-4.50	**$1.90*10^{-5}$**	-0.52	-0.42	-0.37	1.17
Language	Thalamic variability	-0.16	(-0.38, -0.01)	0.09	-1.90	0.06	0.06	-0.19	-0.18	1.71
	PCA dimensionality	-11.19	(-14.80, -6.65)	3.03	-3.69	**$3.73*10^{-4}$**	-0.31	-0.35	-0.35	1.71
Precuneus	Thalamic variability	0.50	(0.14, 0.84)	0.16	3.09	**$2.64*10\text{-}^{3}$**	0.41	0.30	0.27	1.14
	PCA dimensionality	-29.19	(-42.91, -14.54)	8.09	-3.61	**$4.03*10^{-4}$**	-0.44	-0.34	-0.31	1.14
Primary visual	Thalamic variability	0.38	(-0.014, 0.95)	0.21	1.86	0.07	0.39	0.19	0.15	1.25
	PCA dimensionality	-69.08	(-100.17, -48.96)	12.69	-5.44	**$3.93*10^{-7}$**	-0.57	-0.48	-0.45	1.25
Salience (anterior)	Thalamic variability	-0.07	(-0.30, 0.14)	0.10	-0.70	0.49	0.26	-0.07	-0.06	1.63
	PCA dimensionality	-12.78	(-19.00, -8.37)	2.61	-4.90	**$4.0*10^{-6}$**	-0.50	-0.45	-0.43	1.63
Salience (posterior)	Thalamic variability	-0.14	(-0.35, 0.13)	0.10	-1.38	0.17	0.07	-0.14	-0.13	1.32
	PCA dimensionality	-14.37	(-19.93, -9.02)	3.49	-4.12	**$7.90*10^{-5}$**	-0.37	-0.39	-0.39	1.32
Sensorimotor	Thalamic variability	-0.02	(-0.28, 0.17)	0.07	-0.27	0.79	0.04	-0.03	-0.03	1.41
	PCA dimensionality	-1.64	(-4.61, 0.91)	1.56	-1.05	0.30	-0.11	-0.11	-0.11	1.41
Visuospatial	Thalamic variability	0.06	(-0.14, 0.26)	0.10	0.56	0.58	0.33	0.06	0.05	1.55
	PCA dimensionality	-10.08	(-14.23, -6.19)	2.51	-4.02	**$1.16*10^{-4}$**	-0.48	-0.38	-0.36	1.55

Note: Variability difference = within-network cortical variability minus thalamic variability (estimated by $\sqrt{power}$). PCA = principal component analysis; CI = confidence interval; SE = standard error; VIF = variance inflation factor. Significant *p*-values are in bold font. 95% Bootstrap CI was computed via 1000 resamples with replacement of the data. "Zero-order", "partial," and "semi-partial" columns reflect effect sizes in Pearson's correlation metric.

Figures

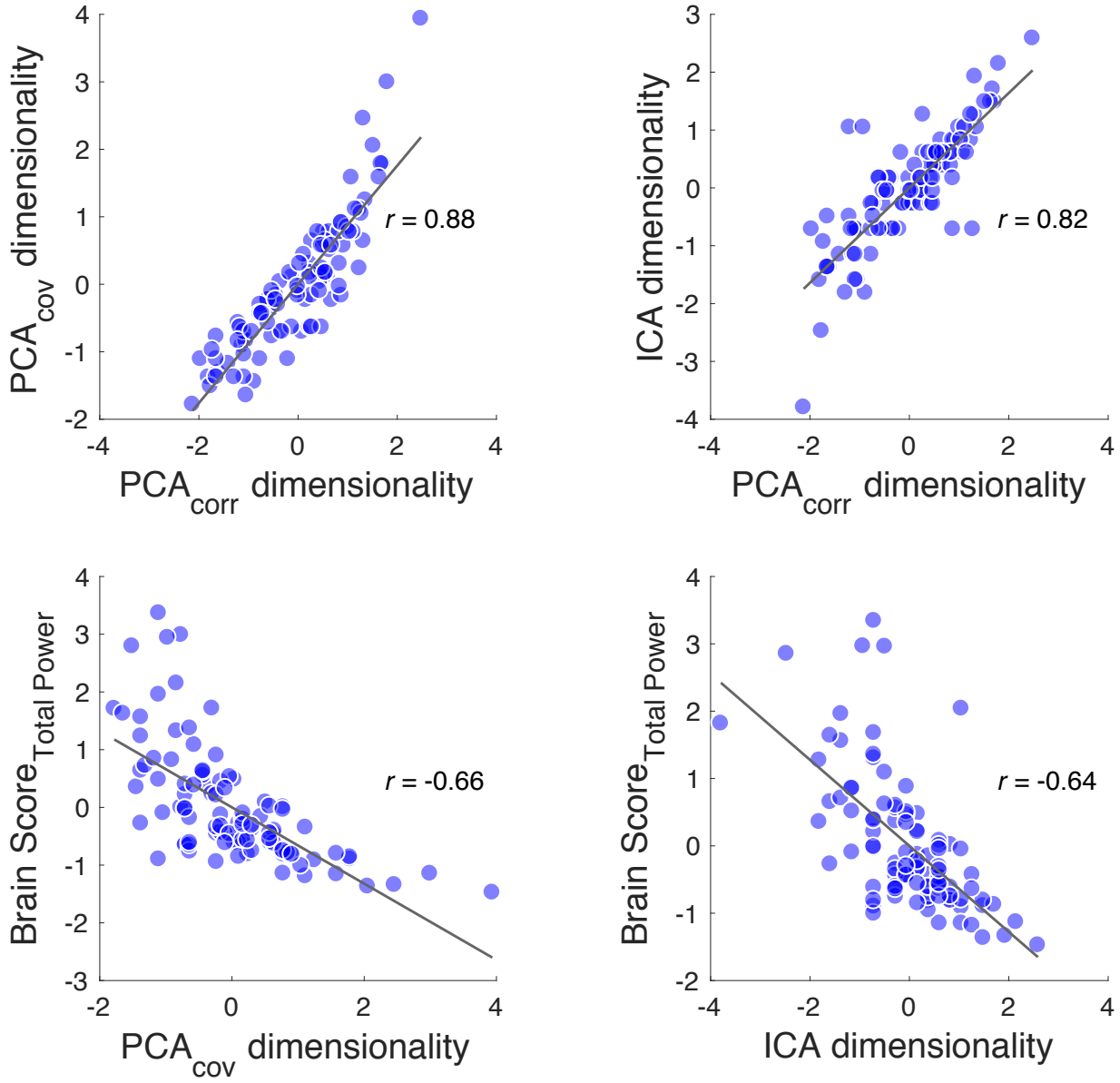

Figure S1: Consistent negative correlations between network dimensionality and local temporal variability across various forms of dimensionality estimation. PCA = principal components analysis; PCA_{covar} = covariance matrix-based PCA; PCA_{corr} = correlation matrix-based PCA; ICA = independent components analysis. Bottom row: Brain $score_{Total\ Power}$ = latent score representing local temporal variability (estimated by $\sqrt{power}$) from separate PLS model runs for PCA_{covar} and ICA-based models. All axis variables are z-transformed.

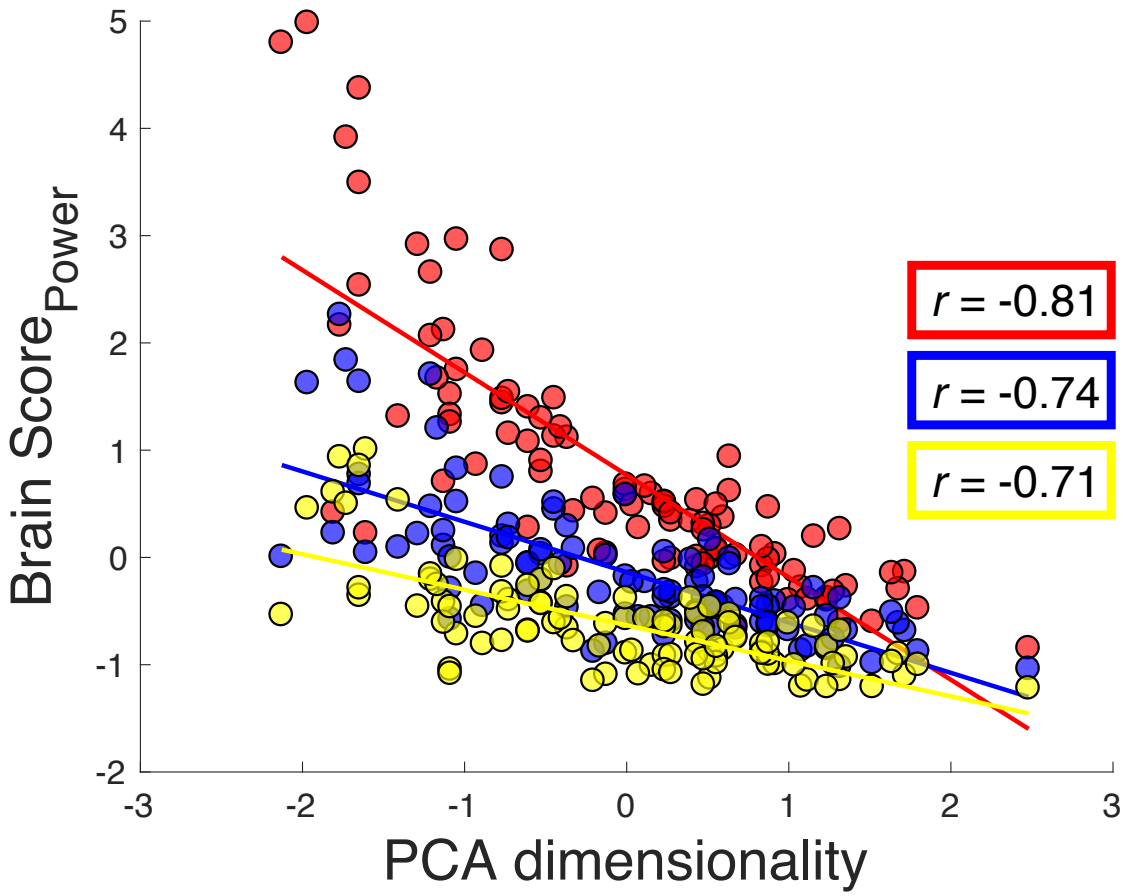

Figure S2: Consistent negative correlations between network dimensionality and local temporal variability across low (red), medium (blue), and high (yellow) frequency power bands. PCA = principal components analysis. Brain score$_{Power}$ = PLS model-derived latent score representing local temporal variability (estimated by $\sqrt{power}$) separately for low, medium, and high frequency ranges. Both axis variables are z-transformed.

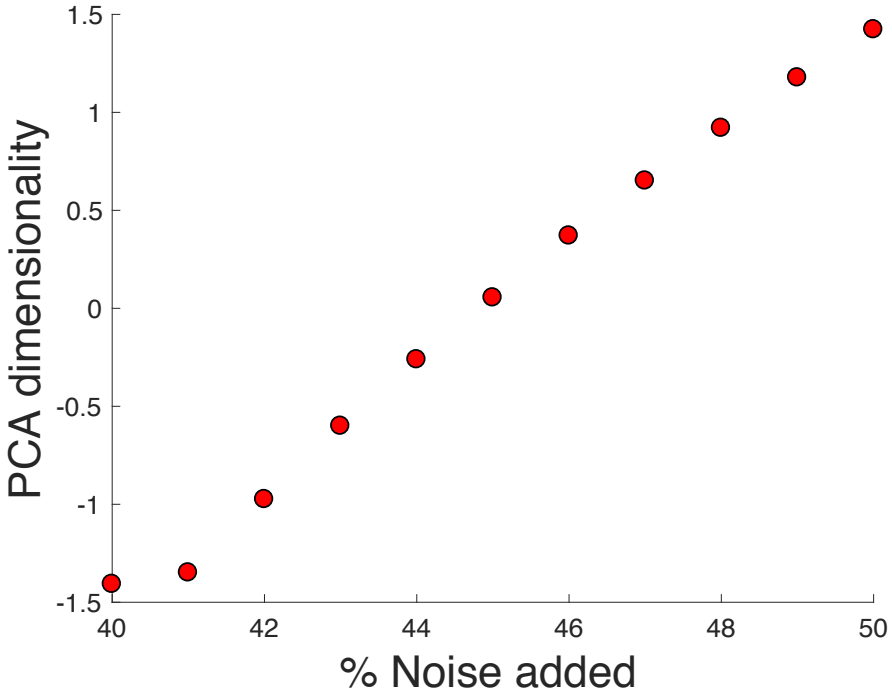

Figure S3: Increasing simulated random noise increases PCA dimensionality. PCA = principal components analysis. % Noise added = the proportion of random noise added to the simulated sine wave amplitude (amplitude = 1), thus reflecting an equivalent proportional increase in total time series variation. Y-axis variable is z-transformed.

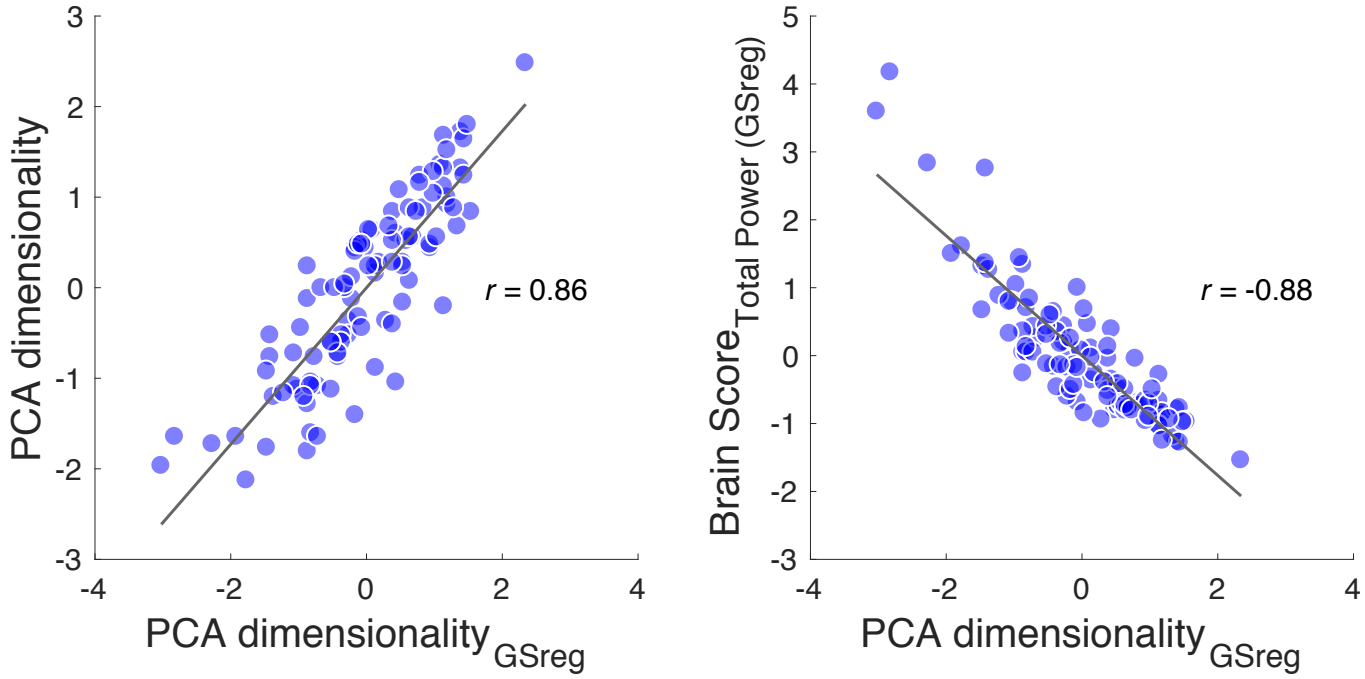

Figure S4: Global signal regression does not affect the relation between network dimensionality and local temporal variability. The left plot shows very similar PCA dimensionality estimates pre and post global signal regression. The right plot shows an equally strong relation between PCA dimensionality and local variability as seen in Figure 1. GSreg = global signal regression. Brain Score$_{\text{Total Power (GSreg)}}$ = PLS model-derived latent score representing local temporal variability (estimated by $\sqrt{power}$) following global signal regression. All axis variables are z-transformed.

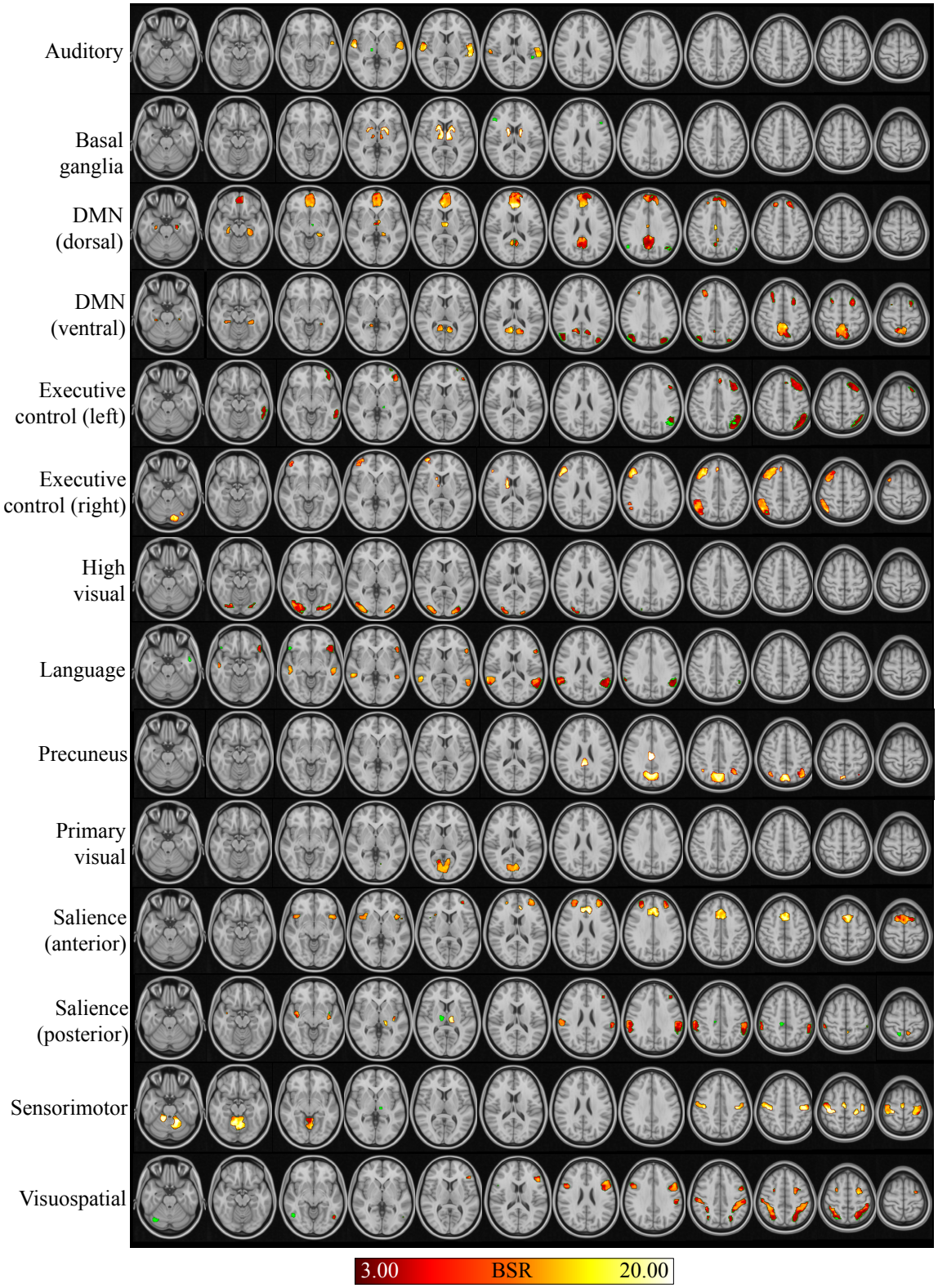

Figure S5: Network-specific, PLS-derived brain plots representing consistent negative correlations between network dimensionality and local signal variability. BSR = bootstrap ratio. Green voxels are those within the *a priori* network mask, but that did not meet the BSR threshold.

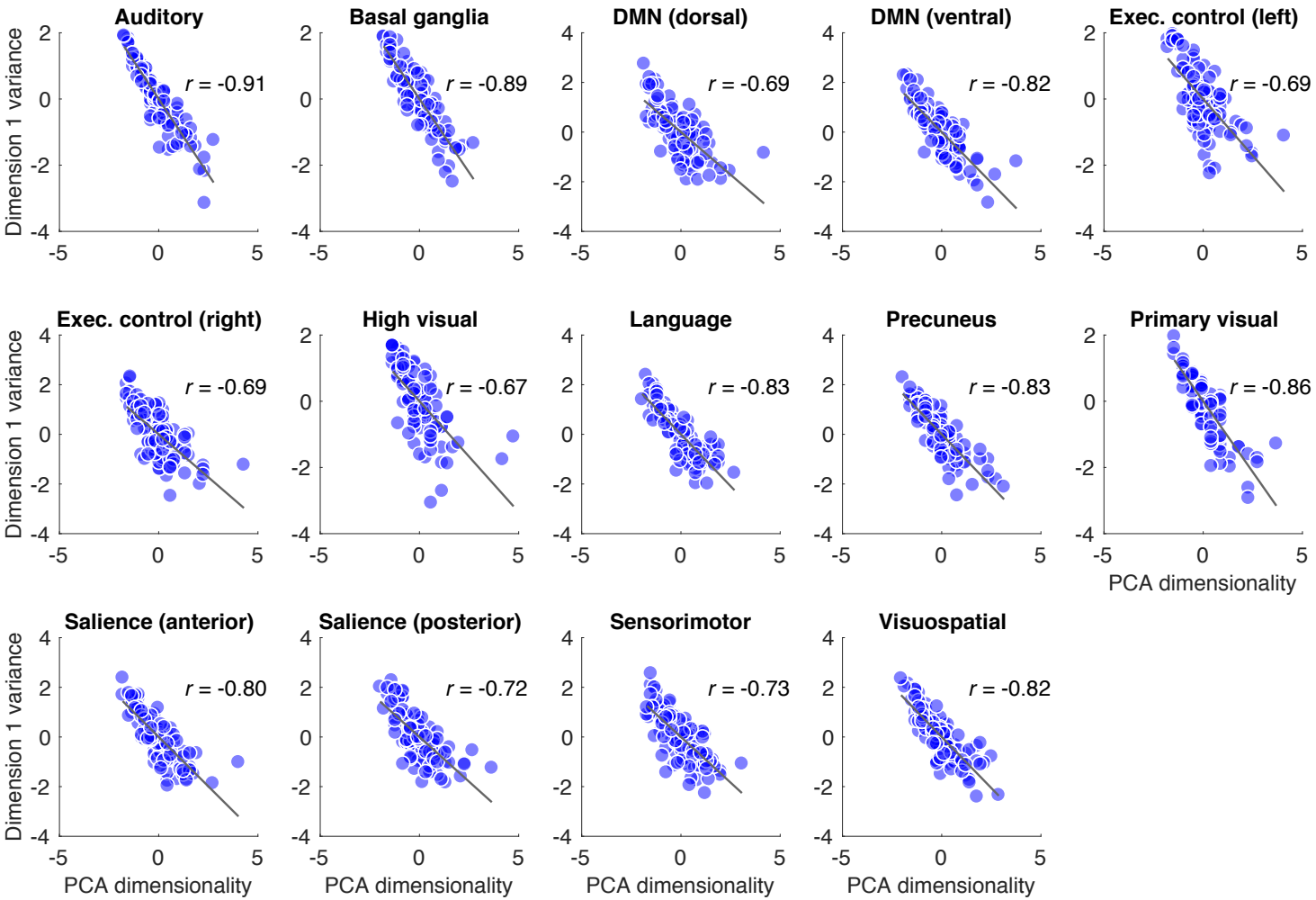

Figure S6: Correlations between PCA dimensionality (90% criterion) and variance accounted for by first component from PCA dimensionality estimation, within-network. All axis variables are z-transformed.

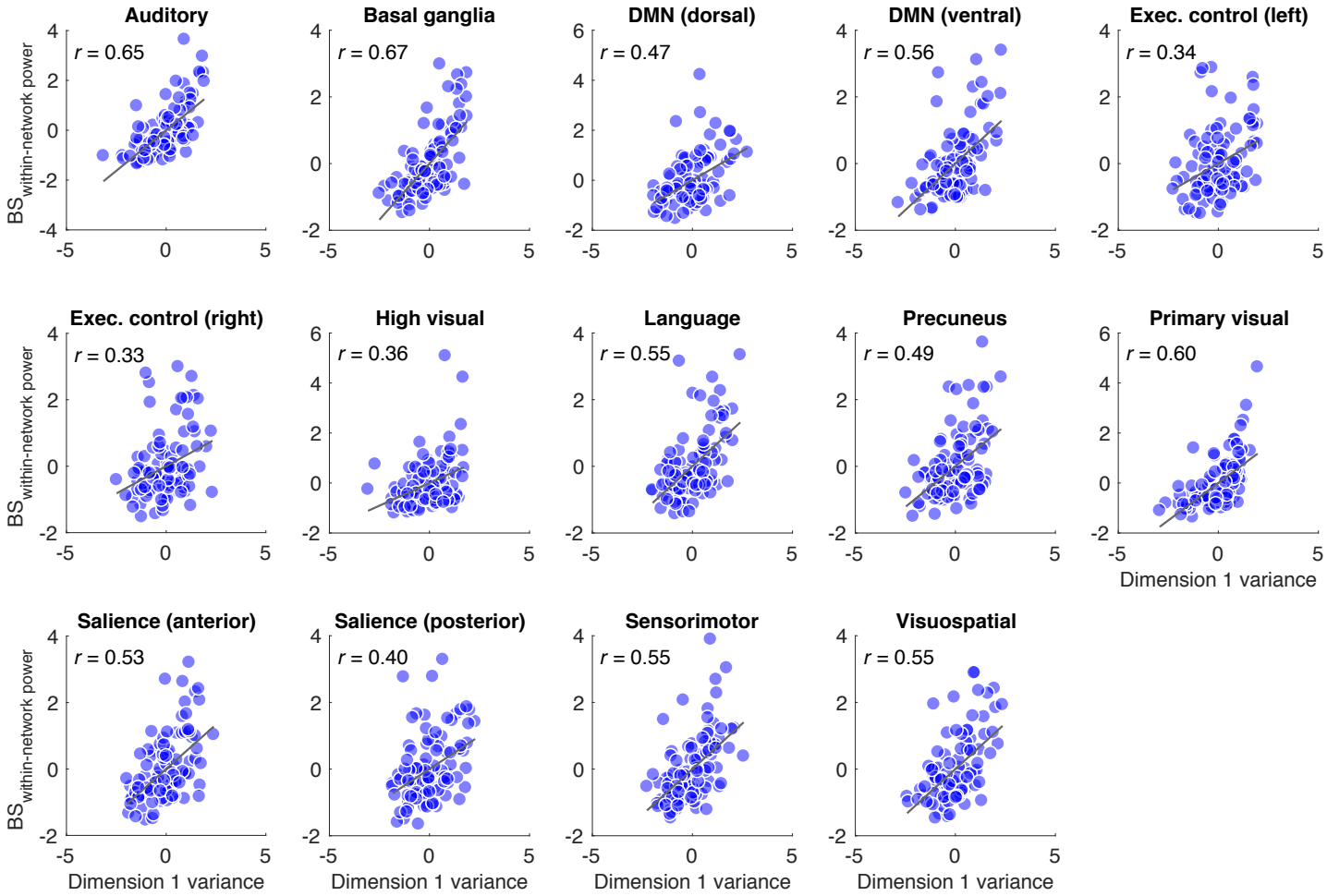

Figure S7: Consistent positive correlations between (i) variance accounted for by the first component from PCA dimensionality estimation and (ii) local signal variability across possible a priori networks of interest. $BS_{\text{Within-Network power}}$ = PLS model-derived latent brain score representing local temporal variability (estimated by $\sqrt{power}$); this brain score is identical to that plotted in Figure 2. DMN = default mode network. All axis variables are z-transformed.